Experimental Mechanics (2015) 55:1339–1352
DOI 10.1007/s11340-015-9994-3

Experimental Study on Crashworthiness of Functionally Graded Thickness Thin-Walled Tubular Structures

F. Xu · X. Tian · G. Li

Received: 21 July 2014 / Accepted: 10 February 2015 / Published online: 20 May 2015

Abstract This paper is an experimental investigation of the crashworthiness behavior of functionally graded thickness (FGT) thin-walled tubular structures. Aluminum alloy AA6061-T5 was chosen because of its high strength to weight ratio and high stiffness. A series of FGT tubes with thicknesses varying linearly from one end to the other were evaluated in quasi-static crushing and three- and four-point bending tests for the purpose of evaluating their energy absorption characteristics. AA6061-T5 FGT tubes with four thickness distributions were considered, namely: t_{top}=0.6, 0.8, 1.0, 1.2 mm, t_{bottom}=1.5 mm. Specific energy absorption (*SEA*) and crush force efficiency (*CFE*) under maximum deformed displacement (δ_{max}) were measured from the tests to infer crashworthiness of the FGT tubes. It was found that the FGT tubes exhibit superior performance relative to a uniform thickness (UT) counterpart especially at the highest displacements and deformed more stably in overall crashing behaviors or collapsed modes. For example, the *CFE* of the AA6061-T5 FGT tube with t_{top}=0.6 mm at δ=80 mm was ~105 %; however, that for an AA6061-T5 UT counterpart with a 1.5 mm thickness tube is only 62 %. This suggests the possibility that crash energy absorption management in ground transportation vehicles may be enhanced through the use of the FGT tube designs.

Keywords Thin-walled tubes · Functionally graded thickness (FGT) · Crushing behavior · Bending performance · Crashworthiness · Energy absorption

F. Xu (✉)
School of Automotive Engineering, Wuhan University of Technology, Hubei Wuhan 430070, China
e-mail: xufx@hnu.edu.cn

F. Xu
Hubei Key Laboratory of Advanced Technology of Automotive Parts, Wuhan University of Technology, Hubei Wuhan 430070, China

X. Tian · G. Li
State Key Laboratory of Advanced Design and Manufacturing for Vehicle Body, Hunan University, Hunan Changsha 410082, China

G. Li
Center for Intelligent New Energy Vehicle, Hunan University, Hunan Changsha 410082, China

Introduction

At present, the requisite balance between improving the crashworthiness efficiency and achieving the light-weight purpose of vehicle structures has increasingly drawn more attention to increasing passenger safety while reducing environmental emissions. Energy absorbing structures that are lightweight and have desirable collapse modes have being been widely utilized and become more and more popular. From the energy absorption point of view, vehicle structures are expected to absorb the maximum generated energy and to minimize the crashing forces transferred from the vehicle structure to the occupants during the impact process. To achieve this purpose, thin-walled tubular structures have been considered to be an effective choice for energy absorption during crash events [1, 2].

Over the past two decades, major effort has been devoted to exploring energy absorption characteristics of thin-walled structures [3–7]. Of the many thin-walled structures, geometrical parameter design for tubular geometries with unique cross sectional shapes had often been used to improve crashworthiness of those thin walled structures such as the prismatic columns with right corners [8–11] and acute/obtuse angles [5]. In addition, the multi-cell or multi-hollow thin-walled structures of square or circle sections in the form of simple

(single cell or hollow), two cell (2×1) and three cells (3×1) have been studied by some researchers. For example, multi-cell square profiles with four small square cells or hollows at each corner of the square were developed by Kim [12] and those obtained results showed dramatic improvements over the conventional square box column in terms of the crashing energy absorption and weight efficiency. Zhang et al. [5, 13–17] investigated the crashworthiness characteristics of multi-cell structures by experimental, theoretical and numerical analyses. However, those different configurations were only explored with uniform thicknesses along the axial direction and single material for the entire tubular structure. It has been verified that the uniform thin-walled structures may not necessarily meet the growing requirements of vehicle light weighting while also guaranteeing the requisite structural crashworthiness [18–20].

Weight reduction without change in functionality of the energy absorption structures can be achieved not only through material substitution, but also through new designs and manufacturing concepts. New advances in tailor-welded blank (TWB) technology allow effective combinations of different materials and different thicknesses to better reduce weight and increase crashworthiness [18–22]. The maximum weight saving could be possibly achieved through intelligent combinations of two or more of light-weight materials and/or discrete thicknesses. As a matter of fact, many automotive companies have been increasingly utilizing TWB technologies by combining various advanced materials with laser processing technology; and then stamping them into such final components products as vehicular B-pillar outer panels [21], floor components [23], front-end (e.g., front longitudinal or side rail) structure [24], door inner panels [25], and other key vehicle components [26]. However, the main defect of those blanks lies in that they consist of discrete thickness sections and may lead to stress concentrations in the weld lines or interfaces which result from the laser welding process [18, 19]. Furthermore, the weld interface may contain complex microstructures with questionable ductility [27–32].

To overcome such defects in a TWB, a relatively new rolling process, named tailor rolled blank (TRB), has been developed [33, 34]. In the newly developed TRB process, the rolling gap can be varied, which leads to a continuous thickness variation in the workpiece. Since the property of variable thickness is achieved by continuous rolling process, any weld interface such as weld line is not introduced. Thus, any energy absorbing tubular structure with continuous graded thickness profiles does not adversely relate to welding processes. Applications of such a rolling process allow reducing more weight compared with traditional stamping or forming processes. As such, varying sheet thickness can better meet more and more demanding design requirements, thereby enhancing utilization of material and/or thickness compared with traditional stamping of a sheet with a uniform thickness. Despite its importance, crashworthiness behavior of functionally graded thickness (FGT) thin-walled structures has nevertheless seldom been reported [35]. More importantly, experimental studies on the potential structures have been not found in the published literatures.

Generally, there are two major considerations in the design of automotive structures for crash energy management: absorption of the kinetic energy of the vehicle and the crash resistance or strength to sustain the crush process and/or maintain passenger compartment integrity [36]. In the crashworthiness design process of vehicle energy-absorbed structures, two kinds of typical crashing events are generally involved and considered. One is the design of a front rail which goes through collapsible folds and is very important to vehicle safety performance (Fig. 1(a)). Another involves side impact which is mainly characterized by bending deformation of a B-pillar (Fig. 1(b)). During those crashing events, energy absorbers allow the vehicle thin-walled structures to maximize absorption of the kinetic energy yielded during the impact process and to minimize the impact forces transferred from vehicle structure to occupants. Therefore, it is important to better understand the crashworthiness including crushing/bending characteristics of the FGT thin-walled structures by taking the thickness variation into account.

For this reason, the motivation of this study is to experimentally explore crushing/bending behaviors and energy absorption of the FGT structures for vehicle crashing applications. In this work, a series of physical tests including quasi-static crushing/bending tests about functionally graded thickness (FGT) thin-walled tubular structures with different thickness

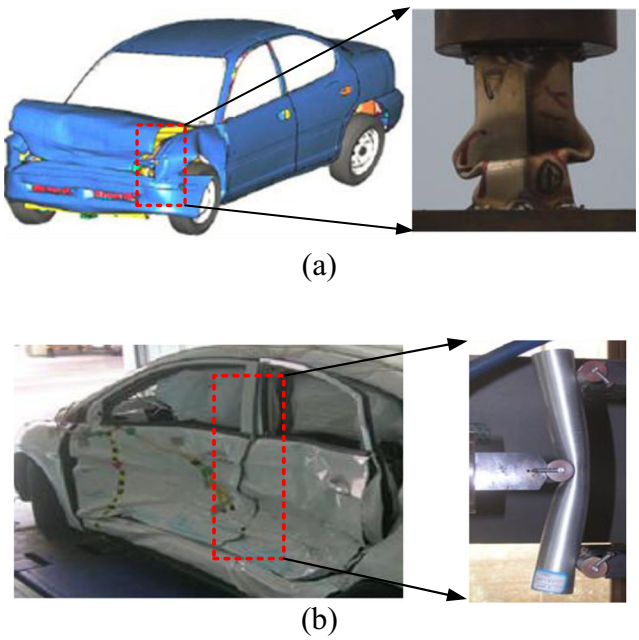

Fig. 1 Two typical crashing events **a** frontal crash [37]; **b** side impact [38]

internals (the difference between maximum thickness value and minimum thickness value, i.e., $\Delta t=t_{max}$-t_{min}) are performed in order to assess energy absorption capacity. The crashworthiness performances of those FGT structures are controlled and changed with the thickness distributions of tube wall. The collapse modes, force versus displacement curves, and energy-absorption characteristics of those FGTs will be explored and examined. The experimental results exhibited the crashworthiness advantages of the FGT tubes with a noticeable improvement in the ability of energy absorption or performance improvements relative to the UT counterpart. For example, for the crushing test, the *CFE* value of the FGT tube with t_{top}/t_{bottom} (or t_{min}/t_{max})=0.6 mm/1.5 mm may improve by 69.4 % with the uniform counterpart at final collapsed displacement. It is also speculated that the improvements in the crushing/bending behaviors are mainly due to the feature of the variable thickness properties. It could be deduced that a better balance should be pursued between the structural lightweight and crashworthiness characteristics through the variation of wall thickness. The primary outcomes of this study provide engineering designers with significant insights into crashworthiness design of those FGTs thin-walled circular tubes, which may facilitate the development of design guidance for such FGT tubes as better energy absorbers.

Experimental Procedure Program

In this section, a series of basic experiments including quasi-static axial crushing and bending tests are conducted on the FGT thin-walled circular tubes with different thickness distributions. The crushing and bending behaviors of the FGT thin-walled tubes are performed using the INSTRON material testing machine (Model 5985, maximum load bearing of 150 kN) for compression or flexure tests, respectively, which allows directly recording the force versus displacement curves.

Material Characteristics

There has been an enormous amount of work performed with these tubular structures with advanced materials such as magnesium alloys [39–42] and advanced high strength steel (AHSS) materials [43, 44]. It is also possible of those materials as energy absorbing tubular structures since they are competitive with common materials such as mild steel. However, the absorbers with aluminum material are still of prime importance in dissipating the impacting energy as they have high strength to weight ratio and high stiffness values [45], which is a primary reason why the aluminum alloy material is chosen herein. Those properties make it a befitting choice for

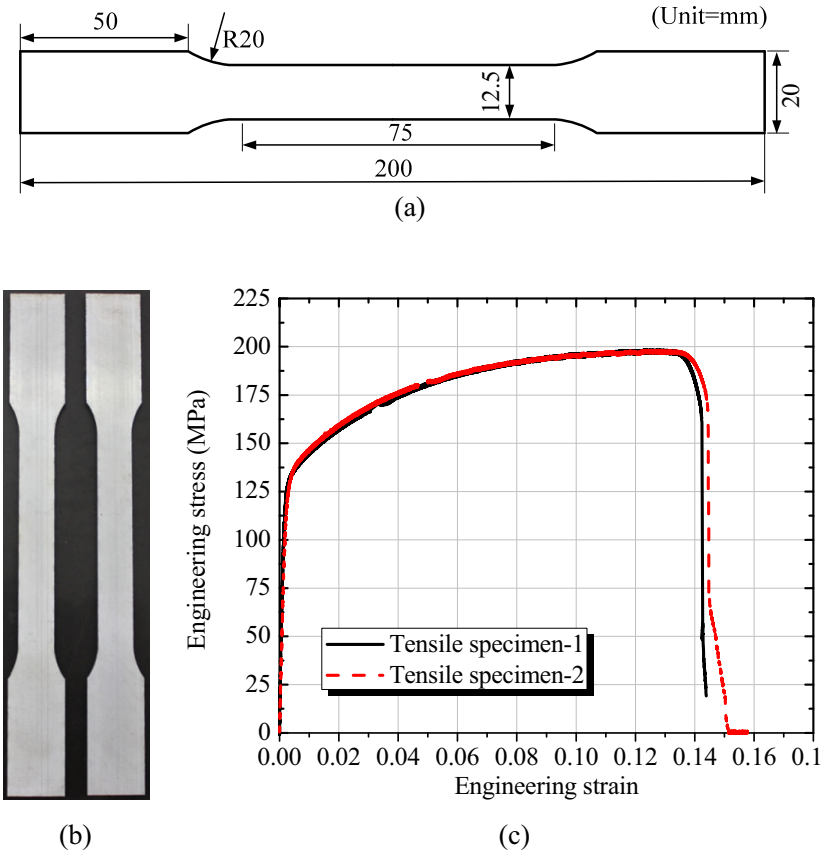

Fig. 2 **a** Standard specimens specified in the ASTM; **b** Tensile coupon test specimen cut off from the circular tube; **c** Engineering stress and engineering strain relationship of metal aluminium material

crash absorbers. The material characteristics of the aluminium material AA6061 T5 were obtained from standard tensile tests on specimens cut from the parent tubes. The dimensions of standard tensile specimens are specified in the ASTM (American Society for Testing and Materials) standard E8M-04 [14]. Figure 2(a) and (b) present the sheet-type standard test specimens. The obtained relationship between the engineering stress and engineering strain of metal aluminium material is illustrated in Fig. 2(c). Several specimens are repetitively performed to show the good consistent results.

Table 1 The description about the linear changes of thickness functional distribution forms for the FGT tubes along the axial direction (Unit: mm)

Cases No.	Top end (x=0)	x=20	x=40	x=60	x=80	x=100	Bottom end (x=120)
1	0.60	0.75	0.90	1.05	1.20	1.35	1.50
2	0.80	0.92	1.04	1.16	1.28	1.40	1.50
3	1.00	1.08	1.16	1.24	1.32	1.40	1.50
4	1.20	1.25	1.30	1.35	1.40	1.45	1.50

Experimental Operation

Although the dynamic behaviors with mandatory and even much higher strain rates are consistent with vehicle impact events [46], the cost from dynamic tests of the components and/or energy-absorbed structures is very expensive and a study on the quasi-static deformation is necessary to qualitatively analyze the collapsed modes and relative performance. Moreover, the utilized and tested aluminium materials are not insensitive to strain rates. Therefore, quasi-static crushing and bending tests of the FGT tubes and the uniform tubes are performed in the work. The tubular members used in this study are constructed with single and uniform material but different thickness distributions. We refer to these as functionally graded thickness (FGT) tubes.

The basic geometry descriptions and experimental configurations of these FGT tubes for axial crushing tests are shown in Fig. 3(a). Those tubes are manufactured by a cutting operation from the counterpart with uniform thickness. The thickness of the crushing (top) end has minimum value and that of the fixed (bottom) end is defined as maximum value. The thickness distributions of all the thin-walled tubes from crushing end to fixed end are linearly arranged along the axial direction. The description about the linear changes of functional distribution forms can be listed in Table 1. Those FGT tubes with four thickness distributions are considered, whose thickness at the initial or top end is 0.6 mm, 0.8 mm, 1.0 mm, and 1.2 mm, respectively. Note that the main discrepancy among those columns lies in the initial thinnest thickness values at the top end. Herein, five types of thin-walled tubes including four FGT tubes and one uniform tube (thickness t=1.5 mm) are considered to compare and understand the crushing behaviors and performance. Each type is performed through two repetitive tests at quasi-static crushing condition of 2 mm/min. The crushing velocity may be such that strain rate effects can be neglected.

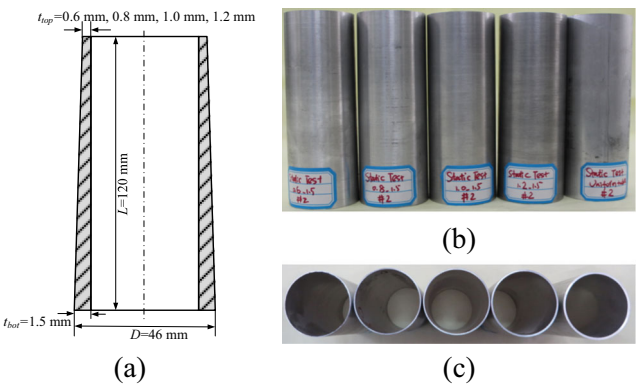

Fig. 3 Schematic configuration of the FGT thin-walled tubes for axial crushing tests, **a** dimensions; **b** side view; **c** top view

Besides of axial crushing characteristics, the bending performance of those FGT structures is evaluated through quasi-static bending experiments in this study. For bending tests, we consider two kinds of deformation modes, i.e., three point bending test and four point bending test to evaluate the bending characteristics and their crashworthiness at a fixed span. Note that the span is a distance between two supports, and span width is defined as a constant of 230 mm (see Fig. 4). The reason of considering the four point bending tests mainly lies in that the crushing objects have often actual width or geometric dimensions. In other words, the contact between the indenters and the tubular structures belongs to surface to surface type in the real side impact. To discuss with simplicity and integration, two kinds of bending modes are investigated in this work. Figure 4 shows the schematic configuration of the FGT thin-walled tubes for both bending tests. Three types of thin-walled tubes including two FGT tubes and one uniform tube are carried out at the INSTRAN testing equipment for bending tests. The indenter is located at the extreme (maximum) thickness or the indentation force is performed at the maximum position. For the three point bending test, three cases of indentation locations are examined, i.e., the indentation end is at the middle location (called as T-case 1), and away from 20 mm (T-case 2) and 40 mm (T-case 3). For the four point bending test, three distances cases between the two indenters are considered: (1) 40 mm (F-case 1); (2) 60 mm (F-case 2); (3) 80 mm (F-case 3). The thickness along the distances between the two indenters is defined to be same and set as a maximum value of 1.5 mm.

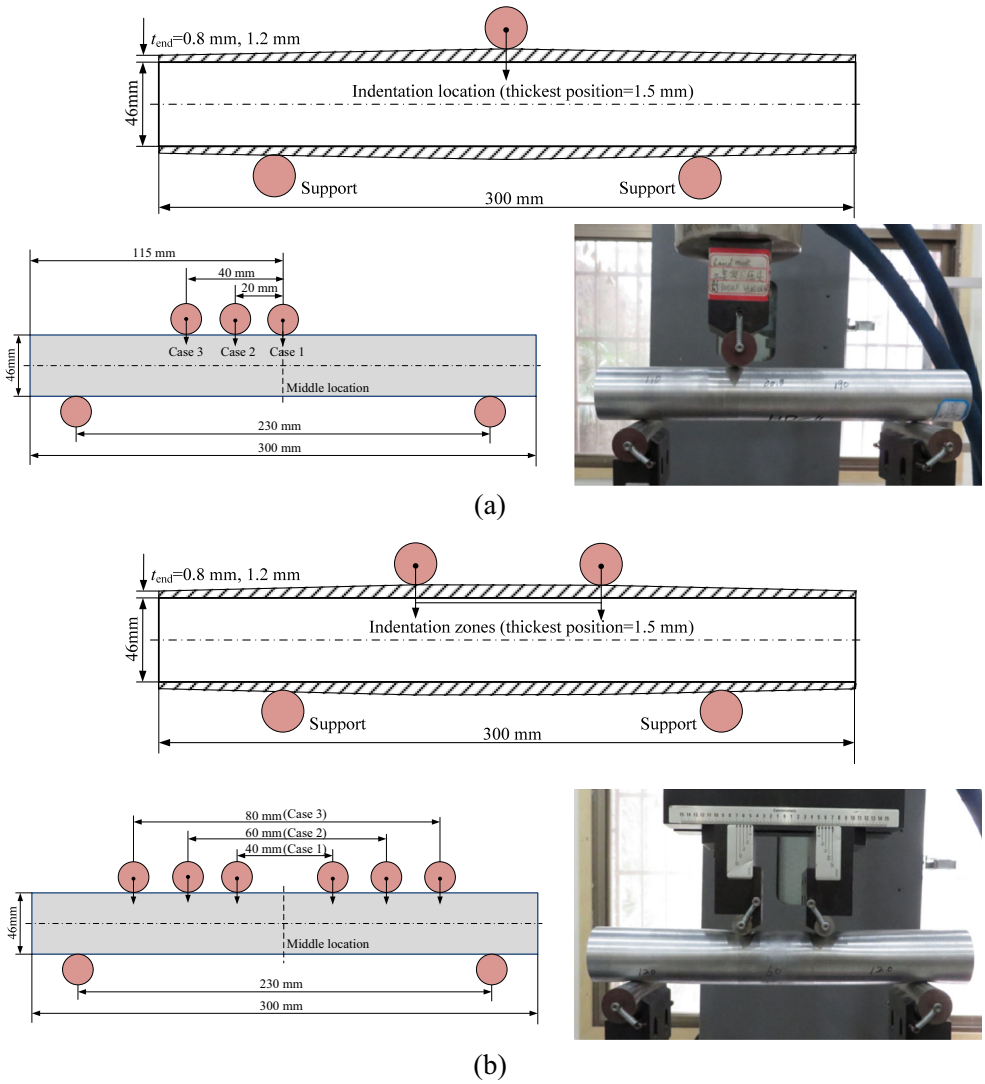

Fig. 4 Schematic configuration of the FGT thin-walled tubes for bending tests, **a** Three point bending; **b** Four point bending

Terminology and Indicators for Crashworthiness

Generally, there are several key indicators to evaluate crashworthiness of a typical energy-absorbed structure. Typically, the total energy absorption (*EA*), specific energy absorption (*SEA*), mean crushing/bending force (F_{mean}), peak force ($F_{\max}$), and crushing/bending force efficiency (*CFE*) are widely used in measuring crashworthiness as given in (equations. (1)-(4)), respectively.

The energy absorption (*EA*) indicates the stable limit of a structure and allows a comparison between different designs. The absorbed energy is determined by integration of the force versus displacement curve.

$$EA = \int_0^{\delta} F(\delta)d\delta \tag{1}$$

where $F(\delta)$ is the instantaneous force corresponding to the displacement δ. The instantaneous load can be obtained from experiments or numerical modeling.

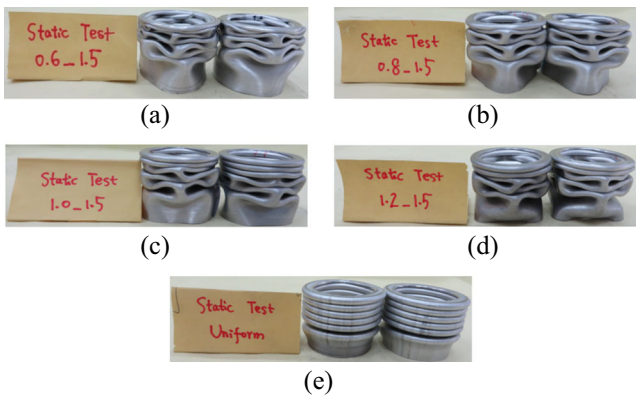

Fig. 5 Final collapsed modes of the FGT and the UT tubes under axial crushing: **a** t_{top}/t_{bottom}=0.6 mm/1.5 mm; **b** t_{top}/t_{bottom}=0.8 mm/1.5 mm; **c** t_{top}/t_{bottom}==1.0 mm/1.5 mm; **d** t_{top}/t_{bottom}==1.2 mm/1.5 mm; **e** t =1.5 mm

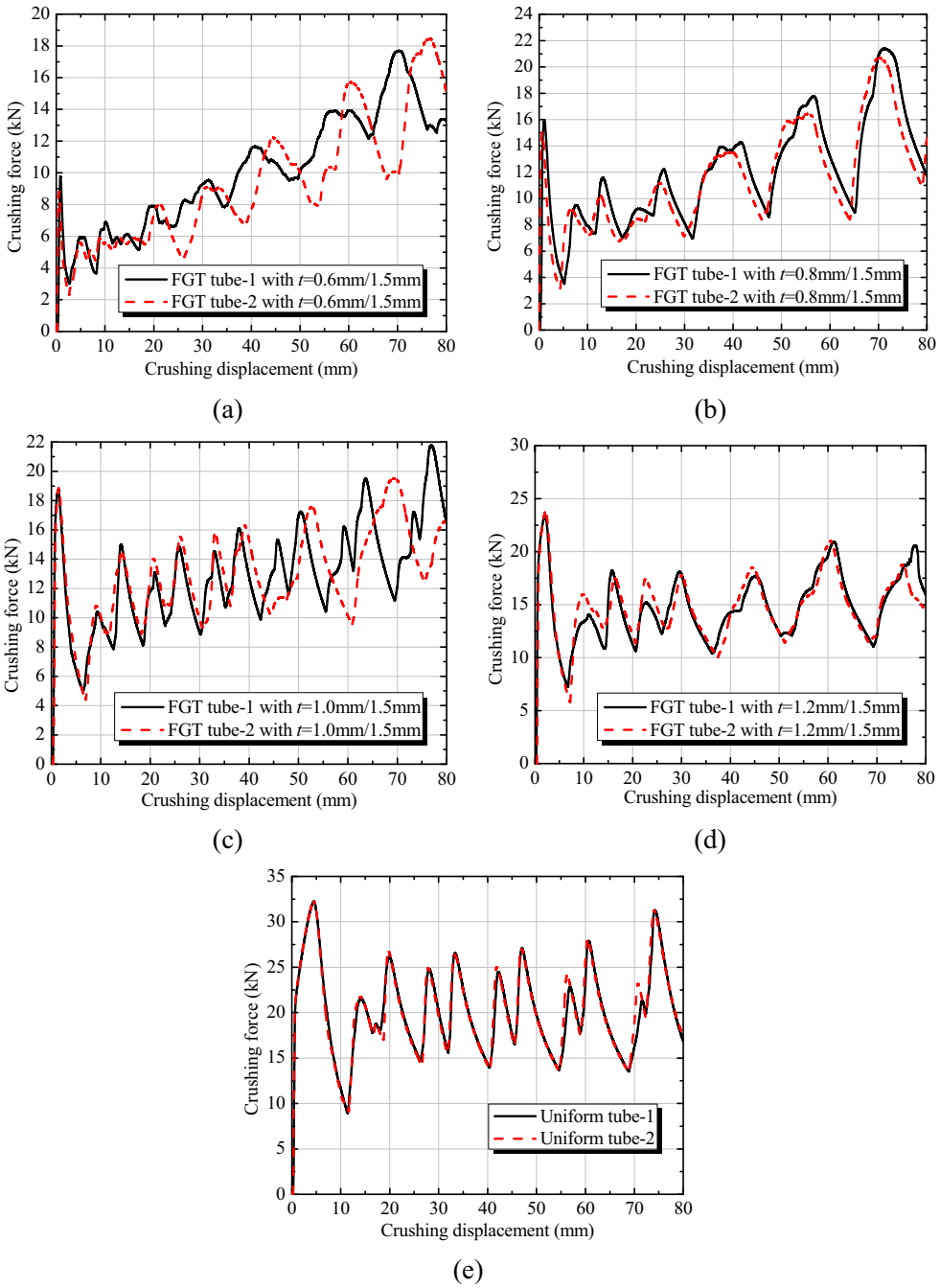

Fig. 6 The histories of crushing force and displacement relationship of the FGT and the UT tubes under axial crushing: **a** FGT tubes with t=0.6 mm/1.5 mm; **b** FGT tubes with t=0.8 mm/1.5 mm; **c** FGT tubes with t=1.0 mm/1.5 mm; **d** FGT tubes with t=1.2 mm/1.5 mm; **e** UT tubes

The specific energy absorption (SEA) assesses the absorbed energy per unit mass of a structure, as follows.

$$SEA = \frac{EA}{m} \tag{2}$$

where m is the total mass of the structure. In this case, a higher value indicates a higher efficiency of material usage.

The mean force for a given deformation indicates capacity of energy-absorption of a structure,

$$F_{mean} = \frac{EA}{\delta} \tag{3}$$

The peak force $F_{\max}$ indicates the force required to initiate collapse and to start the energy absorption process.

The crush/bending force efficiency or namely as the crush force uniformity factor and specific energy absorption can increase simultaneously. It indicates the uniformity of force-displacement curve, meaning that the higher the CFE, the more efficient the structure. Thus, the CFE of a structure is formulated as other key indicator,

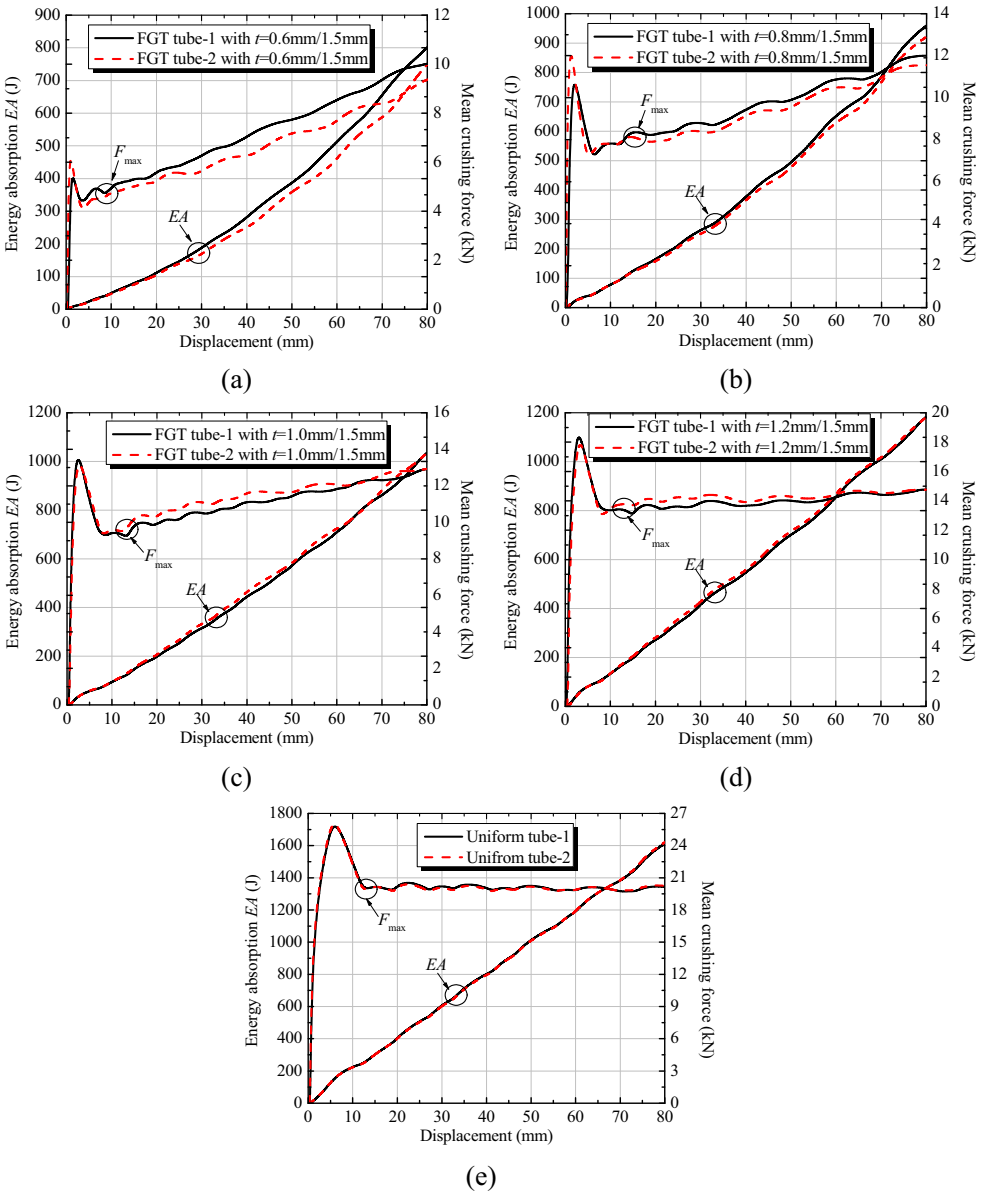

Fig. 7 The relations of energy absorptions *EA* and mean crushing force F_{mean} *vs* displacement for the FGTs with different thickness intervals: **a** FGT tubes with t=0.6 mm/1.5 mm; **b** FGT tubes with t=0.8 mm/1.5 mm; **c** FGT tubes with t=1.0 mm/1.5 mm; **d** FGT tubes with t=1.2 mm/1.5 mm; **e** UT tubes

$$CFE = \frac{F_{mean}}{F_{\max}} \times 100\% \tag{4}$$

Results and Discussions

Results from Quasi-Static Axial Crushing

Crushing Modes and Force & Displacement Curves

In the work, total 10 thin-walled structures including eight FGT tubes and two uniform thickness (UT) tubes are tested. The final deformation modes of all the specimens at final

Table 2 Characteristics indicators for crushing tests of the FGT tubes and the UT tubes with aluminum alloy AA6061 T5

Specimens No.	Mass (g)	F_{imax} (kN)	F_{mean} (kN)	*EA* (J)	*SEA* (J/g)	*CFE* (%)
0.6-1.5-1	46	9.77	10.01	801.56	17.42	102.55
0.6-1.5-2	45	8.81	9.36	749.47	16.65	106.33
0.8-1.5-1	53	15.90	11.99	959.50	18.10	75.43
0.8-1.5-2	52	15.04	11.54	923.48	17.75	76.75
1.0-1.5-1	57	18.74	12.92	1034.07	18.14	68.97
1.0-1.5-2	55	18.85	12.93	1034.43	18.80	68.59
1.2-1.5-1	61	23.45	14.77	1181.68	19.37	62.98
1.2-1.5-2	60	23.79	14.75	1180.28	19.67	62.01
Uniform-1	67	32.23	20.14	1611.20	24.04	62.48
Uniform-2	68	32.21	20.24	1619.65	23.81	62.85

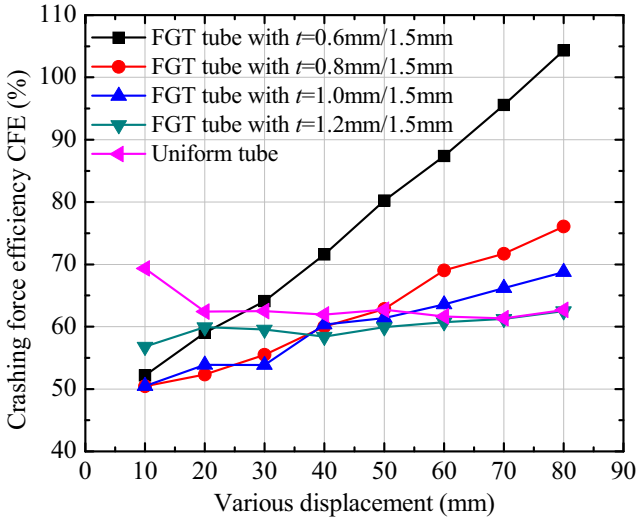

Fig. 8 Comparison of crashing force efficiency (*CFE*) of different FGT tubes under various crushing displacements

collapsed displacement of δ=80 mm are displayed in Fig. 5. Note that no fracture of all these structures is observed at the folding locations based on the obtained collapsed modes. Therefore, it is nearly impossible to determine any information about fracture failure from Fig. 5. Thus, the failure behavior is not considered in this study. It can be clearly seen that the final collapsed modes of the tubes are fairly similar for the same group of specimens, which to a certain extent demonstrates the good repeatability of these tests and consistent results. From the crushed patterns it is also observed that the principal collapse modes are taking either regular progressive folding or irregular (diamond) folding. All the modes are characterized by about six folding lobes. The crush response of the variable thickness tubes differs from that of those tubes with a constant thickness profile. For the considered thin-walled tubes, the uniform tubes collapses more regularly, that is, they undergo through ring mode or concertina mode. Differently, the collapsed modes of the FGT counterpart are characterized by small irregular folds reminiscent of crumpling. In other words, the FGT tubes start to collapse with the ring mode and then switch to the diamond mode, hence exhibiting a mixed mode. The main reason of the variable folding lies in the feature of thickness intervals Δt (thickness value of bottom end or maximum value minus thickness value of top end or minimum value) and depends on the linear variation of thickness along the axial direction. With the increasing of top thickness (minimum value), the deformation modes change from irregular mode to axisymmetric or concertina mode (from Fig. 5(a) to (e)).

Figure 6 shows the relationship between crushing force and displacement of the FGT and the UT tubes under axial crushing, in which both curves are nearly consistent and coincident for the same specimens and show a good repeatability. From those curves, we conclude that the agreement between the two curves becomes worsens (Fig. 6(a)). As a matter of fact, the trivial distinction is inevitable in the real engineering and not artificially controlled. It can be seen that the crushing force of those FGT tubes with the smaller top thickness is eventually increasing after the initial peak crushing force (Fig. 6(a) and (b)). The higher thickness intervals are mainly attributed to the special feature. When the top thickness reaches to a certain extent (Fig. 6(c)-(e)), the axial crushing force shows the relative gentle deformation with the increse of the collasped displacments. An interesting phenomonon is observed that the deformation modes of the FGT tubes show a slight different collapse mechanism from the UT tube. In other words, the FGT tubes have compact collpased changes before the displacement of 30 mm. Thereafter, the collapsed modes demonstrate that the spare changes, i.e., the distance between two peak crushing forces is much longer. Differently, the uniform tubes are crushed with regular progressive folding in the whole process of axial crushing.

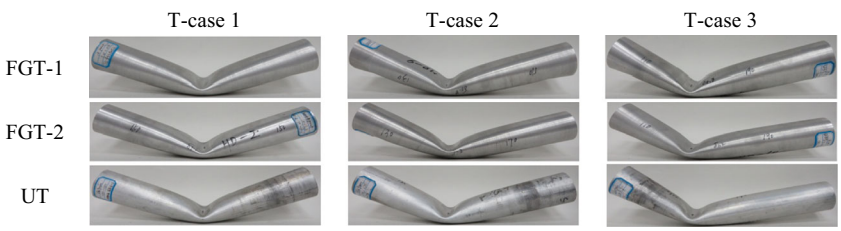

Fig. 9 Final bending modes of the FGT and the UT tubes under three point bending tests

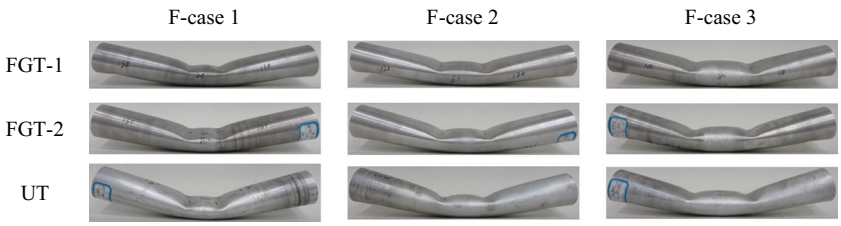

Fig. 10 Final bending modes of the FGT and the UT tubes under four point bending tests

Comparative Analysis of Axial Crushing Characteristics

Based upon the abovementioned direct response data, the relationships of energy absorption and mean crushing force *vs* displacement are illustrated in Fig. 7. It is obviously seen that the energy absorption behaviors with different thickness intervals Δt are rather different from each other. With the increase of thickness at the top end (impact end) (from Fig. 7(a) to (e)), the energy absorptions are increasingly changed with much straighter trends. The reason mainly lies in that the thickness distributions are gradually increasing from top end to bottom end. Moreover, thickness value of top end is bigger and bigger from Fig. 7(a) to (e). For the mean crushing force, the change trends are much flatter with the decreasing of the thickness intervals or increasing of top thickness value.

The experimental data for various crashworthiness criteria for crushing tests of the FGT and the UT tubes are summarized in Table 1. In the naming of the specimens numbers for the FGT tubes, "X-Y-N", the first letter is the minimum thickness value, and Y corresponds to the maximum wall thickness, and N denotes the test number (N=1, 2). The energy absorption (EA) of those tubes was determined from the area under the force-displacement curves up to the final collapse displacement (δ_{max}=80 mm) based on (equation (1)). The energy absorption per weight or the specific energy absorption (SEA) was also calculated through (equation (2)). Herein, the mean crushing force is calculated as EA divided by the final compressive displacement (δ_{max}=80 mm).

From Table 2, the initial peak crushing forces of the FGT tubes is much lower than those of the uniform counterpart. Moreover, the decreased range is significant with the decrease of top thickness. The mean crushing force, total and specific energy absorption have the same characteristics as the initial peak crushing force. Although those indicators of the FGT tubes are not so advantageous with those of the uniform tubes, the crushing force efficiency (CFE) of the FGT tubes is much higher than that of the uniform counterpart. The CFE measures the uniformity of force-displacement curve of the crushing process. Higher value indicates a more ideal energy absorption characteristic. Those results may provide indicative design information for engineers to achieve relatively higher energy absorption capacity of the FGT tubes. It can be shown that the improvements of those FGT tubes are mainly due to the thickness distributions of top end, which demonstrates that graded structures are in general much more efficient than those with single or well-distributed thickness.

To further analyze the characteristics of these FGT tubes, the comparisons of crushing force efficiency of different FGT tubes under variable crushing displacements are illustrated in Fig. 8. Obviously, the CFE of the UT tubes is a little higher

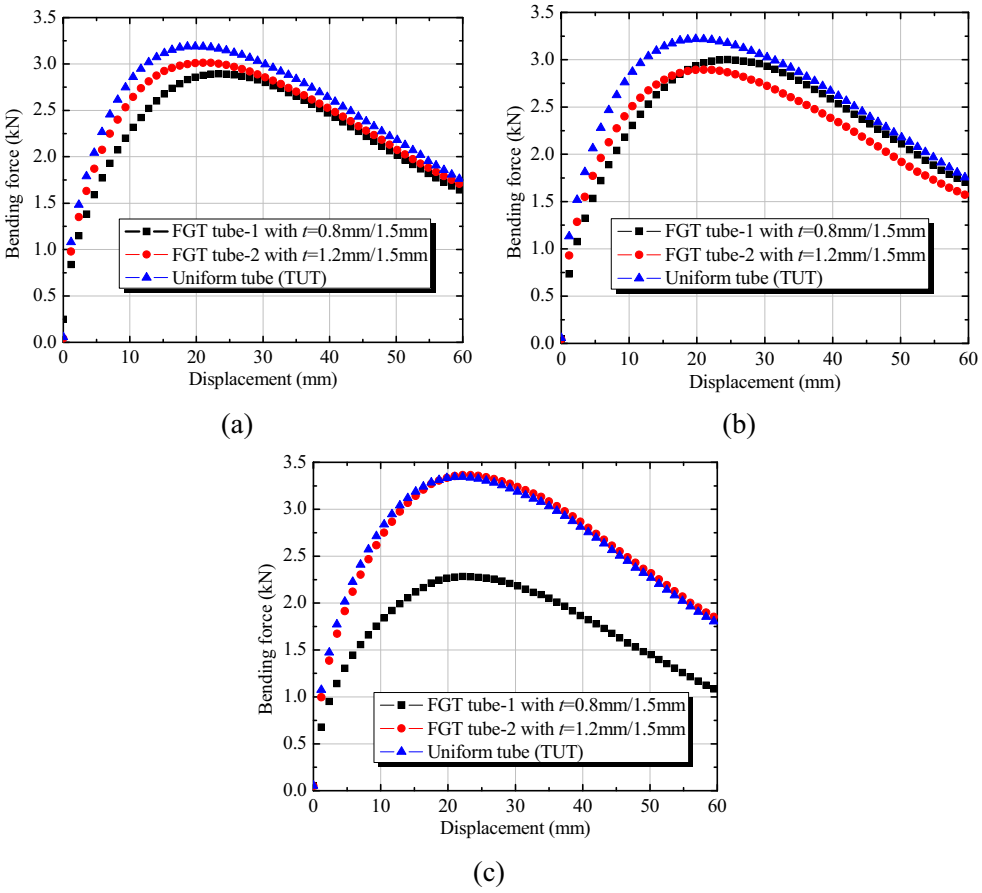

Fig. 11 Bending force and displacement relationship of the FGT and the UT tubes under three point bending tests: **a** T-case 1; **b** T-case 2; **c** T-case 3

than that of those FGT tubes at initial crushing stage (less than 20 mm). However, the advantages of graded structures are more and more obvious with the crushing displacements increasing especially when the deformation distance is more than 60 mm. It is also seen that the *CFE* value of the FGT tubes is much higher than that of the uniform tubes (about 62 %). For the FGT tube with t_{top}/t_{bottom}=0.6 mm/1.5 mm, the *CFE* increases linearly with the increase of collapsed deformations and may be far higher than 100 % and achieves to about 105 %. Thus, the performance of graded structures (t_{top}/t_{bottom}=0.6 mm/1.5 mm) could improve by 69.4 % relative to a uniform tube. The main reason can be attributed to the higher mean crashing force than the initial crashing force. Alternatively, the *CFE* of a uniform tube nearly changes only very minimally. In other words, the crushing performance of the UT tubes does not depend on variable collapsed displacements due to the uniform thickness profile along the axial direction.

Results from Bending Tests

The quasi-static bending tests of the FGT thin-walled structures were experimentally carried out to obtain bending modes, force & displacement relationship, and other performance indicators so as to evaluate and compare their crashworthiness characteristics under the transverse bending loading. The transverse loading is often expected in a crash event especially when the side-impact system combined by the vehicle door and B-pillar is collapsed with involving the bending deformations.

Bending Modes and Force & Displacement Curves

In general, three deformation modes of simply supported circular tubes under the action of the transverse loading by an indenter were identified by Thoms et al. [47]: (1) Pure crumpling or twist mode when only the top local surface of the tube initially deformed; (2) Combined bending and crumpling mode when further crumpling of the specimen combined with bending between the supports; (3) Structural collapse mode when large rotations at the two ends of the tube occurred about the centre under the indenter after the maximum load has been reached. In this study, the latter two typical modes can be found.

Figures 9 and 10 showed the final bending modes of all the specimens tested including those FGT and UT tubes at three cases under the three and four point bending tests, respectively. It seems as if they underwent some similar plastic deformations between the FGT and the UT tubes for the same case. Note that no fracture failures are observed for all the collapsed

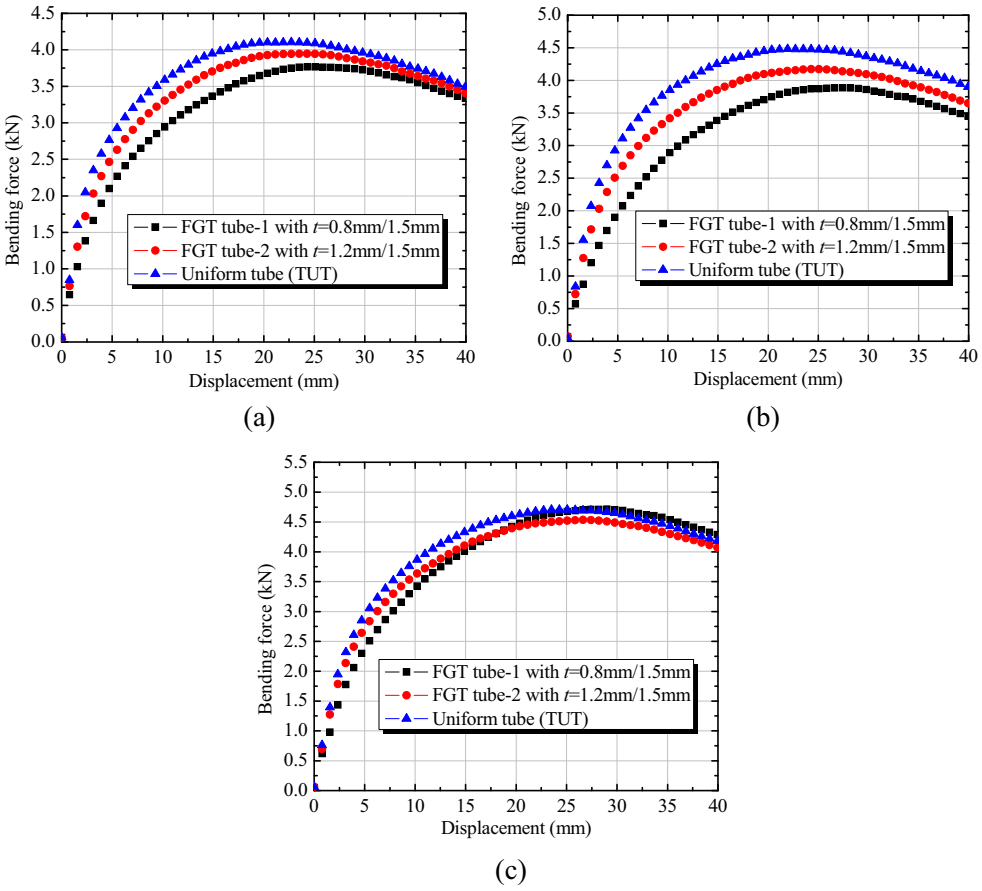

Fig. 12 Bending force and displacement relationship of the FGT and the UT tubes under four point bending tests: **a** F-case 1; **b** F-case 2; **c** F-case 3

Table 3 Characteristics indicators for bending tests of the FGT tubes and the UT tubes

Specimens No.	Thickness (mm)	Mass (g)	F_{max} (kN)	*EA* (J)	*SEA* (J/g)
Three point bending					
T-C1-F1	0.8/1.5	122	2.89	137.55	1.12
T-C1-F2	1.2/1.5	145	3.01	145.14	1.00
T-C1-T	1.5	158	3.19	153.70	0.97
T-C2-F1	0.8/1.5	119	3.01	141.48	1.18
T-C2-F2	1.2/1.5	140	2.89	137.30	0.98
T-C2-U	1.5	157	3.22	154.95	0.98
T-C3-F1	0.8/1.5	111	2.29	105.43	0.94
T-C3-F2	1.2/1.5	147	3.37	159.96	1.08
T-C3-U	1.5	159	3.35	159.60	1.00
Four point bending					
F-C1-F1	0.8/1.5	133	3.77	126.04	0.94
F-C1-F2	1.2/1.5	147	3.95	135.25	0.92
F-C1-U	1.5	158	4.11	142.85	0.90
F-C2-F1	0.8/1.5	125	3.89	127.02	1.01
F-C2-F2	1.2/1.5	146	4.17	141.86	0.97
F-C2-U	1.5	158	4.49	155.14	0.98
F-C3-F1	0.8/1.5	138	4.72	153.36	1.11
F-C3-F2	1.2/1.5	146	4.53	153.24	1.04
F-C3-U	1.5	157	4.71	160.49	1.02

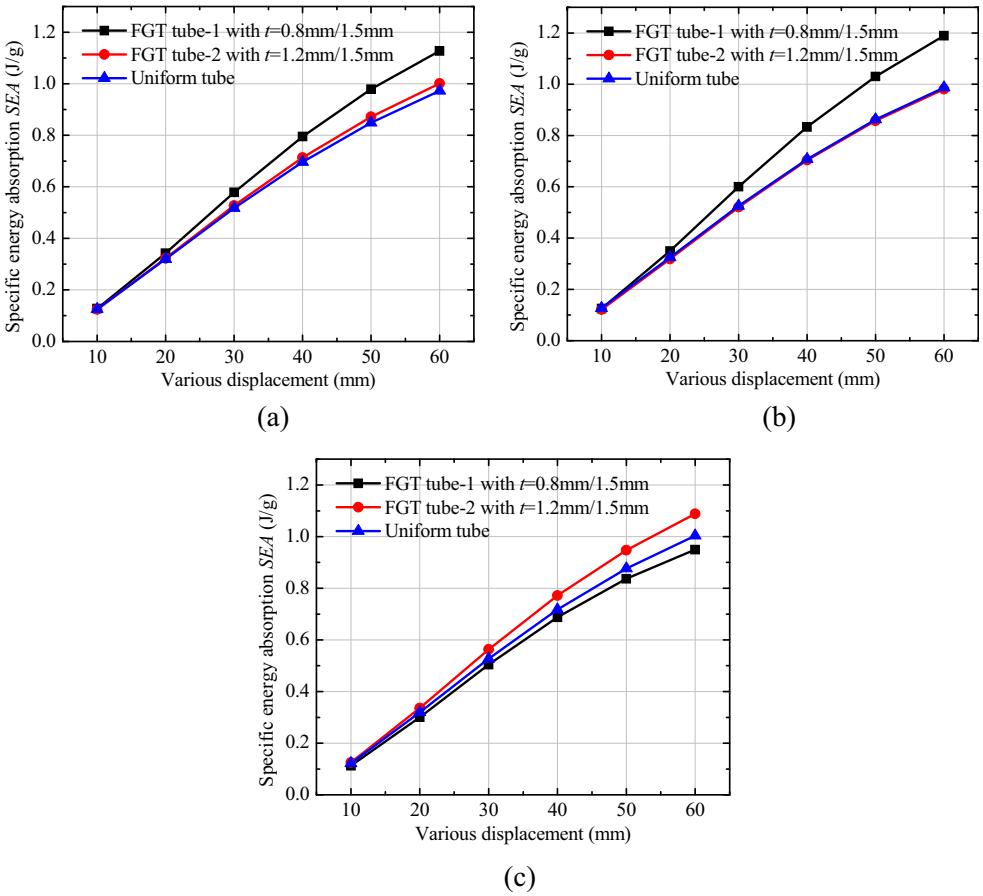

Fig. 13 Comparisons of specific energy absorption of different FGT tubes under different bending displacements (Three point bending): **a** T-case 1; **b** T-case 2; **c** T-case 3

modes. For those empty structures, bending stiffness increases with wall thickness of the tubes. Higher bending resistance usually causes structures to undergo through less twist and more bending at the similar indentation displacements. For the FGT tubes, the bending stiffness is not uniform due to their various thickness distribution profiles. At the indenter location in which the wall thickness has a maximum value, it seems to be the highest bending stiffness.

Figures 11 and 12 give the bending force-displacement relationships of the FGT and the UT tubes under the three and four point bending tests. From Fig. 11, when the indenter is located at the middle of specimens (T-case 1) and away from 20 mm (T-case 2), the uniform tubes have a much higher peak crushing force due to the thicker and uniform thickness value of the entire structures. However, as the distance away from the middle location is up to 40 mm (T-case 3), the force and displacement relationship of the FGT tube with t_{top}/t_{bottom}= 1.2 mm/1.5 mm has almost the same change trend as that of a uniform counterpart. As a matter of fact, for an actual side impact event, the crashing location is often not at the middle of B-pillar, but at some a position underneath the thin-walled structure. Thus, from the view point of crashworthiness and light-weight, the FGT tubes seem as the more effective and ideal energy absorbers. In addition, with the increasing of indenter spans, these three different tubes have a better consistent (Fig. 12(c)). It demonstrates again that the FGT tubes with weight reduction but without change in functionality of the energy-absorbed structures are superior to the uniform structures through varying thickness.

Comparative Analysis of Bending Characteristics

The performance indicators for bending tests of the FGT tubes and the UT tubes are listed in Table 3. In the naming of the specimens numbers for those FGT tubes from the bending tests, as "X-CM-FN/ X-CM-U", the first letter X is either a "T" for a "three point bending", or a "F" for a "four point bending", CM denote the cases (C) of indentation locations (M=1, 2, 3), and then FN correspond to the two different FGT tubes (N=1, 2), e.g., T-C2-F1 indicates the case 2 of the FGT tube-1 with 0.6 mm/1.5 mm under the three point bending. Likewise, U denotes the uniform thickness tube, and others are same as the previous mentioned, e.g., F-C2-U represents the case 2 of the uniform tube under the four point bending. From Table 3, it can be observed that F_{max} of the FGT tubes are obviously a little lower than that of those UT tubes under the three point bending. The *SEA*s between the FGT and the UT tubes are similar, but total weights of the former thin-

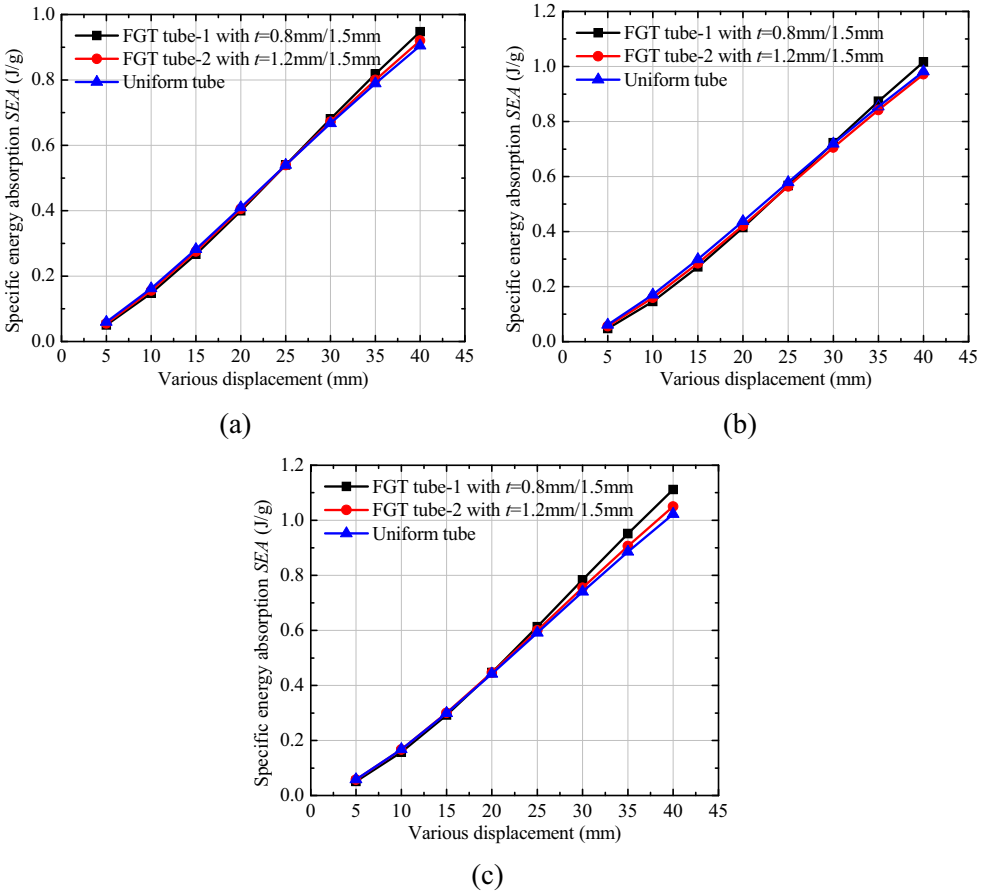

Fig. 14 Comparisons of specific energy absorption of different FGT tubes under different bending displacements (Four point bending): **a** F-case 1; **b** F-case 2; **c** F-case 3

walled structures are much lighter. Therefore, by varying thickness distributions form, the tubes can achieve similar crashworthiness characteristics as the equivalent thickness structures.

In addition, the comparisons of specific energy absorption (*SEA*) of different FGT tubes under different bending displacements are also shown in Figs. 13 and 14. For all the cases of three bending tests, the *SEA*s of the FGT tubes are superior to the uniform tubes especially when the bending distances are eventually increasing. Additionally, T-case 2 which the indenter is 20 mm away from the middle location seems to be higher energy absorption per total weight (Fig. 13(b)). For the three cases of the four point bending tests, similar trends between the graded and uniform tubes can be observed from Fig. 14. However, there are slight improvements for the FGT tubes with an increase of bending displacements especially for F-case 3 when the distance is more than 30 mm (Fig. 14(c)). Note the total mass of the FGT tubes in this work is much smaller than that of a uniform counterpart. Therefore, for total energy absorptions, it can be speculated that the indicator of the FGT tubes is much higher than that of a uniform counterpart under the same mass. Thus, a better balance can be pursued between the structures lightweight and crashworthiness characteristics through the various thickness properties.

Concluding Remarks

From a series of quasi-static axial crushing and bending tests of functionally graded thickness (FGT) thin-walled circular tubes, the crashworthiness characteristics of the FGT thin-walled structures have been experimentally identified in the paper. The work provides some experimental data for the FGT energy-absorption structures. The effects of different thickness intervals on the crushing and bending characteristics are evaluated. The deformation modes and force-displacement relationships are compared for all the FGT structures with various thickness intervals ($\Delta t = t_{max}$-t_{min} or $t_{botttom}$-t_{top}). For bending behavior, three different indenter positions are considered to enable comparison of the bending performance. Other associated crashworthiness criteria, such as initial peak force, mean crushing force, specific energy absorption, and crushing force efficiency are then examined and compared with each other. It is found that the FGT structures provide a better balance between these different crashworthiness criteria. The test results demonstrated the advantages of the FGT tubes with a noticeable improvement in terms of energy absorption and peak force, especially when the deformation displacements are eventually increasing. It is suggested that the crashworthiness behaviors can be further improved to some extent by devising different thickness distributions. For example, the *CFE* value of the FGT tube with t_{top}/t_{bottom}=0.6 mm/1.5 mm achieves to about 105 % and is much higher than that of a uniform tubes (about 62 %). These observations suggest that graded tubes have the potential to be very efficient energy absorptions structures in vehicle crash events.

Note that only the aluminium material was utilized in this work. Other advanced materials such the advanced high strength steels (AHSS) and magnesium alloys are also of importance to the automotive industry since their successful development may lead to further vehicle weight reduction, reduced fuel consumption and enhanced occupant protection. Further studies should be experimentally focused on the crashworthiness of the FGT tubes with the abovementioned promising materials so as to understand the crashing/bending performance of different individual or combined materials.

Acknowledgments This work is supported by The National Natural Science Foundation of China (61232014) for providing financial support.

References

1. Wierzbicki T, Abramowicz W (1983) On the crushing mechanics of thin-walled structures. J Appl Mech 50:727–734
2. Abramowicz W, Wierzbicki T (1989) Axial crushing of multicorner sheet metal columns. J Appl Mech 56:113–120
3. Ghamarian A, Abadi MT (2011) Axial crushing analysis of end-capped circular tubes. Thin-Walled Struct 49:743–752
4. Song J, Chen Y, Lu G (2012) Axial crushing of thin-walled structures with origami patterns. Thin-Walled Struct 54:65–71
5. Zhang X, Zhang H (2012) Experimental and numerical investigation on crush resistance of polygonal columns and angle elements. Thin-Walled Struct 57:25–36
6. Jones N (2011) Structural impact, 2nd edn. Cambridge University Press, Cambridge, UK
7. Lu G, Yu T (2003) Energy absorption of structures and materials. Elsevier, Woodhead Publishing Limited
8. Zhao H, Abdennadher S (2004) On the strength enhancement under impact loading of square tubes made from rate insensitive metals. Int J Solids Struct 41:6677–6697
9. DiPaolo B, Tom J (2006) A study on an axial crush configuration response of thin-wall, steel box components: the quasi-static experiments. Int J Solids Struct 43:7752–7775
10. Gu G, Xia Y, Zhou Q (2012) On the fracture possibility of thin-walled tubes under axial crushing. Thin-Walled Struct 55:85–95
11. Reddy T, Al-Hassani S (1993) Axial crushing of wood-filled square metal tubes. Int J Mech Sci 35:231–246
12. Kim H-S (2002) New extruded multi-cell aluminum profile for maximum crash energy absorption and weight efficiency. Thin-Walled Struct 40:311–327
13. Zhang X, Zhang H (2014) Axial crushing of circular multi-cell columns. Int J Impact Eng 65:110–125
14. Zhang X, Zhang H (2013) Energy absorption of multi-cell stub columns under axial compression. Thin-Walled Struct 68:156–163
15. Zhang X, Zhang H, Wen Z (2014) Experimental and numerical studies on the crush resistance of aluminum honeycombs with various cell configurations. Int J Impact Eng 66:48–59
16. Zhang X, Zhang H (2012) Numerical and theoretical studies on energy absorption of three-panel angle elements. Int J Impact Eng 46: 23–40

17. Zhang X, Huh H (2010) Crushing analysis of polygonal columns and angle elements. Int J Impact Eng 37:441–451
18. Song Y, Hua L (2014) Influences of thickness ratio of base sheets on formability of tailor welded blanks. Procedia Eng 81:730–735
19. Arman Khan VVN (2014) Satya suresh, srinivasa prakash regalla. Effect of thickness ratio on weld line displacement in deep drawing of aluminium steel tailor welded blanks. Procedia Mater Sci 6:401–408
20. Feistauer EE, Bergmann LA, Barreto LS, Santos JF (2014) Mechanical behaviour of dissimilar friction stir welded tailor welded blanks in Al–Mg alloys for Marine applications. Mater Des 59:323–332
21. Pan F, Zhu P, Zhang Y (2010) Metamodel-based lightweight design of B-pillar with TWB structure via support vector regression. Comput Struct 88:36–44
22. Shi Y, Lin Z, Zhu P, Han S (2008) Impact modeling of the weld line of tailor-welded blank. Mater Des 29:232–238
23. Hariharan K, Kalaivani K, Balachandran G (2012) Foil optimization in tailor welded blank of an automotive floor component. Mater Manuf Process 27:936–942
24. Pan F, Zhu P (2011) Lightweight design of vehicle front–end structure: contributions of multiple surrogates. Int J Veh Des 57:124–147
25. Shin J-K, Lee K-H, Song S-I, Park G-J (2002) Automotive door design with the ULSAB concept. using structural optimization. Struct Multidiscip Optim 23:320–327
26. Davies R, Grant G, Smith M, Oliver E (2000) Formability and fatigue of aluminum tailor welded blanks. SAE Trans: J Mater Manuf 109: 911–918
27. Tao H, Tong W, Hector LG Jr, Zavattieri PD (2008) Uniaxial tensile and simple shear behavior of resistance spot-welded dual-phase steel joints. ASME J Manuf Sci Eng 17:517–534
28. Tong W, Hector LG Jr, Dasch C, Tao H, Jiang XQ (2007) Local plastic deformation and failure behavior of Nd:YAG laser welded AA5182- O and AA6111-T4 sheet metals. Metall Mater Trans A 38:3063–3086
29. Marya M, Wang K, Hector LG Jr, Gayden XH (2006) Tensile-shear forces and fracture modes in single and multiple weld specimens in dual-phase steels. J Manuf Sci Eng 128:287–298
30. Hector LG Jr, Chen YL, Agarwal S, Briant CL (2004) Texture characterization of autogenous Nd:YAG laser welds in AA5182-O and AA6111-T4 aluminum alloys. Metall Mater Trans A 35(9):3032–3037
31. Agarwal S, Briant CL, Hector LG Jr, Chen YL (2007) Friction stir processed AA5182-O and AA6111-T4 aluminum alloys. Part 1: electron backscattered diffraction analysis. J Mater Eng Perform 16(4): 391–403
32. Hector LG Jr, Chen YL, Agarwal S, Briant CL (2007) Friction stir processed AA5182-O and AA6111-T4 aluminum alloys. Part 2: tensile properties and strain field evolution. J Mater Eng Perform 16(4): 404–417
33. Yang RJ, Fu Y, Li G, Application of tailor rolled blank in vehicle front end for frontal impact. SAE Technical Paper 2007-01-0675
34. Chuang C, Yang R, Li G, Mallela K, Pothuraju P (2008) Multidisciplinary design optimization on vehicle tailor rolled blank design. Struct Multidiscip Optim 35:551–560
35. Cengiz B, Merve T (2014) Energy absorption of circular aluminium tubes with functionally graded thickness under axial impact loading. Int J Crashworthiness. doi:10.1080/13588265.2014.982269
36. Savic V, Passive pedestrian protection approach for vehicle hoods. SAE Technical Paper 2014-01-0513.
37. Fang H, Rais-Rohani M, Liu Z, Horstemeyer MF (2005) A comparative study of metamodeling methods for multiobjective crashworthiness optimization. Comput Struct 83(25–26):2121–2136
38. Kang CY, Seo JW, Kim JH, Joo YB (2013) Ultra high strength steel b Pillar reinforcement structure to enhance Side impact and roof crash as reducing weight. In: Proceedings of the FISITA 2012 world automotive congress, Springer, pp. 53–71
39. Lugo M, Jordon JB, Solanki KN, Hector LG Jr, Bernard JD, Luo AA, Horstemeyer MF (2013) Role of different material processing methods on the fatigue behavior of AZ31 magnesium alloy. Int J Fatigue 52:131–143
40. Marya M, Hector LG Jr, Verma R, Tong W (2006) Microstructural effects of AZ31 magnesium alloy on its tensile deformation and failure behaviors. Mater Sci Eng A 418(1–2):341–356
41. Carter JT, Melo AR, Savic V, Hector Jr LG, Krajewski PE. Structural evaluation of an experimental aluminum/magnesium decklid. SAE Technical Paper 2011-01-0075
42. Savic V, Hector LG Jr, Kim S, Verma R (2010) Local mechanical properties of a magnesium hood inner component formed at elevated temperature. ASME J Eng Mater Technol 132(021006):1–10
43. Hector Jr LG, Krupitzer R, Sachdev AK (2013) Integrated Computational Materials Engineering (ICME) for third generation advanced high-strength steels: a new four-year project. Proceedings of the Int. symposium on new developments in advanced high-strength steels, Vail, CO, pp. 341–349, AIST, Warrendale
44. Coryell J, Savic V, Hector Jr LG, Mishra S. Temperature effects on the deformation and fracture of a quenched-and-partitioned steel. SAE Technical Paper 2013-01-0610.
45. Krajewski PE, Hector LG Jr, Qi Y, Mishra RK, Sachdev AK, Bower AF, Curtin WA (2011) Atoms to autos: a multi-scale approach to modeling aluminum deformation. JOM 63:24–32
46. Yang X, Hector LG Jr, Wang J (2014) A combined theoretical/experimental approach for reducing ringing artifacts in low dynamic testing with servo-hydraulic load frames. Exp Mech 54: 775–789
47. Thomas S, Reid S, Johnson W (1976) Large deformations of thin-walled circular tubes under transverse loading—I: an experimental survey of the bending of simply supported tubes under a central load. Int J Mech Sci 18:325–333